Electronic Supplementary Information (ESI)

Fluorene Core Based Electron Acceptor for Fullerene-Free BHJ Organic Solar Cells – Towards Power Conversion Efficiency Over 10%

Table of Contents

General Experimental Details

S1. Methods and materials

Materials: 2,7-Bis-(4,4,5,5-tetramethyl-1,2,3-dioxaborolan-2-yl)9,9-bis(2-ethylhexyl)fluorene (BAF-BA_2) and 4,7-bromobenzo[*c*][1,2,5]-thiadiazole (BT-Br_2) and dicyano-n-hexylrhodanine were prepared according to published procedures.[1] All the starting chemicals and reagents for synthesis were purchase from commercial sources and used without further purification. Fluorene, [$Pd(PPh_3)_4$], [$Pd(dppf)Cl_2$] and 2-ethyl hexyl bromide were purchased from Sigma-Aldrich and used as received. Bispinacolatodiborane was purchased from AlfaAesar. Solvent were dried and purified using standard techniques under nitrogen atmosphere. Reactions were carried out in an inert nitrogen atmosphere. All products were purified by using column chromatography on silica gel (60-120 mesh and 100-200 mesh).

General methods: All compounds were characterized by Nuclear magnetic resonance (NMR), Fourier transform infrared (FT-IR) spectroscopy and Matrix-assisted laser desorption/ionization-time-of flight mass spectrometry (MALDI-TOF MS) spectrometry spectroscopy.^{1}H NMR and ^{13}C NMR spectra were recorded on Bruker AV-400 spectrometer and AV-300 spectrometer instrument with tetramethylsilane (TMS) as internal standard at 298 K. UV-Vis absorption spectra of molecules in solution were recorded on a UV-1601 Shimadzu UV-Vis spectrometer. The cyclic Voltammogram (CV) were measured by using a three-electrode cell with a Pt wire working electrode, a Pt mesh counter electrode, and a saturated calomel (SCE) reference electrode in saturated KCl aqueous solution, 0.1 M tetrabutylammonium perchlorate (TBAP) as the supporting electrolyte in dry CH_2Cl_2 solution with a scan speed of 0.1 $V \cdot s^{-1}$. All UV and CV measurements were carried out at room temperature.

S2. Synthetic Procedures

Synthesis and characterization of **FRdCN$_2$***:* The synthetic steps of **FRdCN$_2$** molecules is illustrated in **Scheme S1** (ESI). BAF-BA$_2$ was cross coupled with 5-(7-bromobenzo[*c*] [1,2,5]thiadiazole-4-yl)furan-2-carboxaldehyde (BT-F-CHO) groups using Suzuki cross coupling reaction afforded the aryl dialdehyde intermediate (BAF-2CHO). A strong electron withdrawing group dicyano-N-hexylrhodanine was introduced as terminal acceptor units via Knoevenagel condensation reaction yielded **FRdCN$_2$** as dark red solid. **FRdCN$_2$** is highly soluble in common organic solvents (12 mg/mL) like DCM, THF and chloroform at room temperature. Purity of all intermediate and final molecule was confirmed by NMR, FT-IR spectroscopy and MALDI-TOF MS spectrometry. Results are shown in **Figure S1-S8**.

5-(7-bromobenzo[c][1,2,5]thiadiazole-4-yl)furan-2-carbadehyde (BT-F-CHO):

A solution of BT-Br$_2$ (1 g, 3.40 mmol) , 5-formyl furan-2-boronic acid (0.475 g, 3.06 mmol), K_2CO_3 (2M Solution 5 mL), in THF (30 ml) was degassed for 30 minutes before addition of [Pd (PPh_3)$_4$] (10 mg) and subsequent degassing for 10 min. The reaction mixture was heated under nitrogen at 80 °C for 24 hrs and progress of reaction was observed by TLC. After cooling to room temperature, the reaction was quenched with water and extracted with CH_2Cl_2 and dried over Na_2SO_4 and filtered. After removing solvent the desired compound was purified by column chromatography with hexane/ethyl acetate, affording pure compound **BT-F-CHO** in 56% yield (0.580 g, 1.876mmol). ^{1}H NMR (500 MHz, $CDCl_3$), δ ppm: 9.75-9.74 (s, 1H), 8.16-8.14 (d, J=7.78Hz, 1H), 7.97-7.94 (d, J=7.6Hz, 1H) 7.89-7.87 (d, J=3.81Hz, 1H), 7.44-7.42 (d, J=3.81Hz, 1H). ^{13}C NMR (100 MHz, $CDCl_3$), δ ppm: 177.45, 154.13, 152.05, 132.2, 129.42, 126.23, 125.92, 123.65, 122.37, 115.39, 114.61.

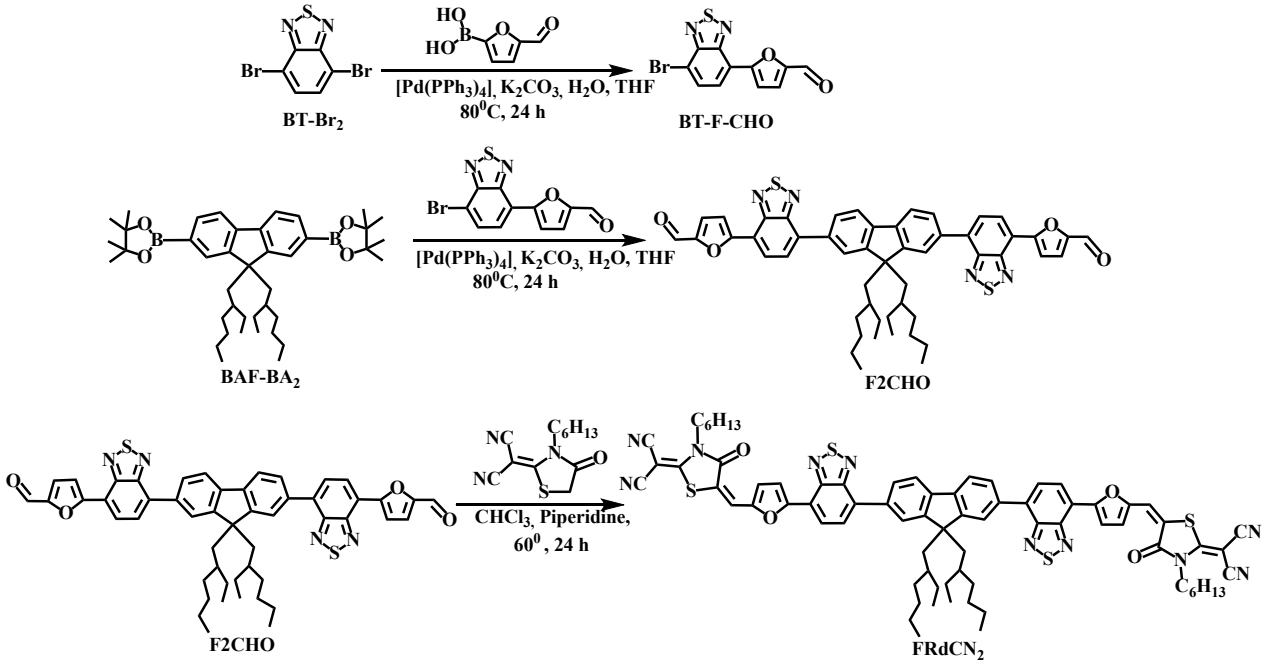

Scheme S1. Synthetic route of **$FRdCN_2$.**

F2CHO:

A mixture of BAF-BA_2 (0.500 g, 0.778mmol) , BT-F-CHO (0.601 g, 1.94 mmol), K_2CO_3 (2M Solution 5 mL) and THF (20 ml) were added to a 100 ml of two neck round bottom flask. The mixture was degassed before addition of [Pd (PPh_3)$_4$] (10 mg) and subsequent degassing for half hour. The reaction mixture was refluxed under nitrogen at 80 °C for 24 hrs. After cooling to room temperature, the reaction was quenched with water and extracted with CH_2Cl_2. Organic layer was dried over Na_2SO_4. After removing the solvent the desired product was purified by column chromatography with hexane/ethyl acetate, affording brown color semisolid product **F2CHO** in 53% yield (0.350 g, 0.413mmol). ^{1}H NMR (500 MHz, $CDCl_3$), δ ppm: 9.76-9.75 (s, 2H), 8.42-8.40 (d, J=7.47Hz, 2H), 8.08-8.03 (m, 4H), 7.97-7.91 (m, 6H), 7.89-7.86 (d, J=7.47Hz, 2H), 2.21-2.14 (m, 4H),0.99-0.85 (m, 20H), 0.59-0.56(t, J=6.8Hz, 12H). ^{13}C NMR (75 MHz, $CDCl_3$), δ ppm: 177.69, 155.25, 154.01, 151.93, 151.87, 151.41, 141.50, 135.82, 128.49, 127.40, 126.44, 125.21, 120.11, 114.12, 44.5, 34.76, 33.86, 28.14, 27.10, 22.15, 13.95, 10.36. FT-IR

(KBr) (cm^{-1}): 3414, 2921, 2860, 1726, 1673, 1543, 1462, 1388, 1340, 1261, 1218, 1021, 813, 770, 436,406. MS (MALDI-TOF-MS): m/z calcd for $C_{51}H_{50}N_4O_4S_2$ 847.10; $[M]^+$, found 846.35.

FRdCN$_2$:

Under nitrogen atmosphere a mixture of dicyano-N-hexylrhodanine (0.231 g, 0.920 mmol) and F-2CHO(0.200 g 0.230mmol), piperidine (2 drops) were dissolved in chloroform (30 ml) in a 50 ml of two neck round bottom flask and then the mixture was heated at 60^0C for 24 hrs. After completion of reaction the reaction mixture was allow to cool up to room temperature, the reaction was quenched with water and extracted with CH_2Cl_2 and the crude product was purified by flash column chromatography on silica gel (CH_2Cl_2) to yield **FRdCN$_2$** as a dark red solid in 32% yield (0.110 g, 0.084mmol). ^{1}H NMR (400 MHz, $CDCl_3$), δ ppm: 8.23-8.19 (d, J=7.45Hz, 2H), 8.18-8.13 (m, 2H), 8.08-8.03 (m, 2H), 8.01-7.91 (m, 6H), 7.76-7.73 (s, 2H), 7.20-7.16 (d, J=3.67Hz, 2H), 4.29-4.20 (t, J=7.70Hz, 4H), 2.23-2.17 (d,4H), 1.82-1.75 (m, 4H), 1.67-1.20 (m, 26H), 0.93-0.89 (t, J=6.84Hz, 12H), 0.75-0.71 (m, 2H), 0.62-0.58 (t, J=6.84Hz, 6H), ^{13}C NMR (125.77 MHz, $CDCl_3$), δ ppm: 166.38, 166.06, 154.10, 153.49, 152.08, 141.68, 137.99, 135.54, 132.28, 131.35, 128.74, 127.49, 124.58, 124.22, 120.51, 119.08, 113.02, 112.07, 56.42, 55.61, 45.40, 40.14, 31.79, 31.23, 29.54, 29.42, 29.25, 29.22, 25.62, 24.02, 22.58, 22.40, 14.04, 13.92. FT-IR (KBr) (cm^{-1}): 3416, 2922, 2857, 2211, 1716, 1604, 1531, 1458, 1383, 1338, 1206, 1166, 1125, 1024, 899, 804, 728, 576, 520. MS (MALDI-TOF-MS): m/z calcd for $C_{75}H_{76}N_{10}O_4S_4$ 1309.73; $[M]^+$, found 1309.69.

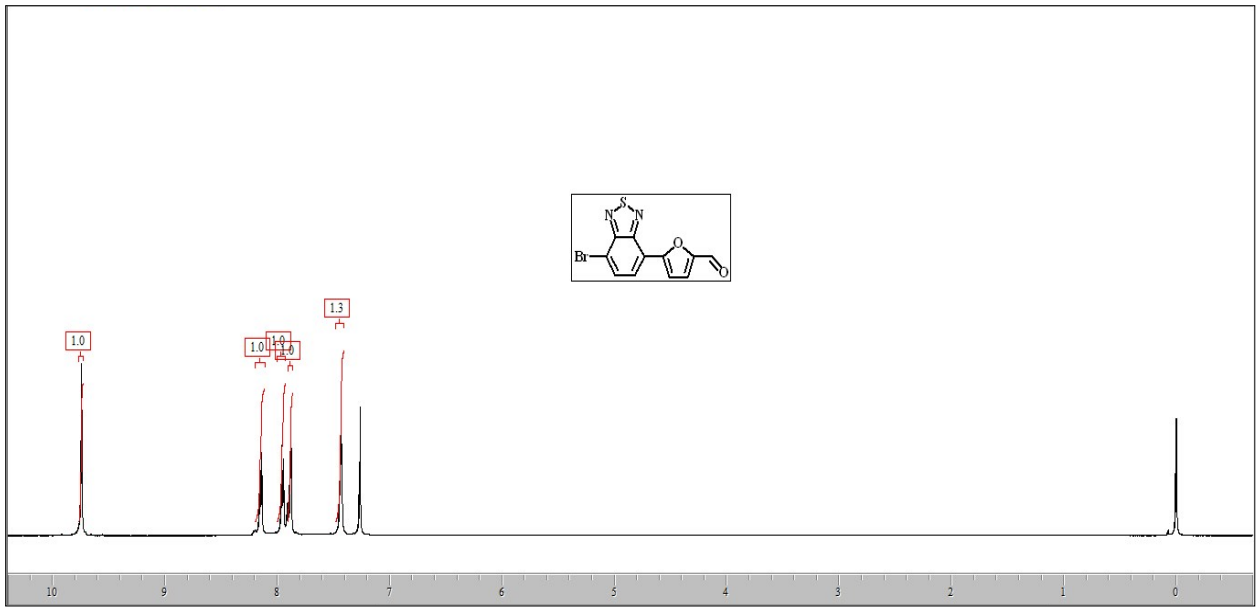

Figure S1. ^{1}H NMR of BT-F-CHO in $CDCl_3$.

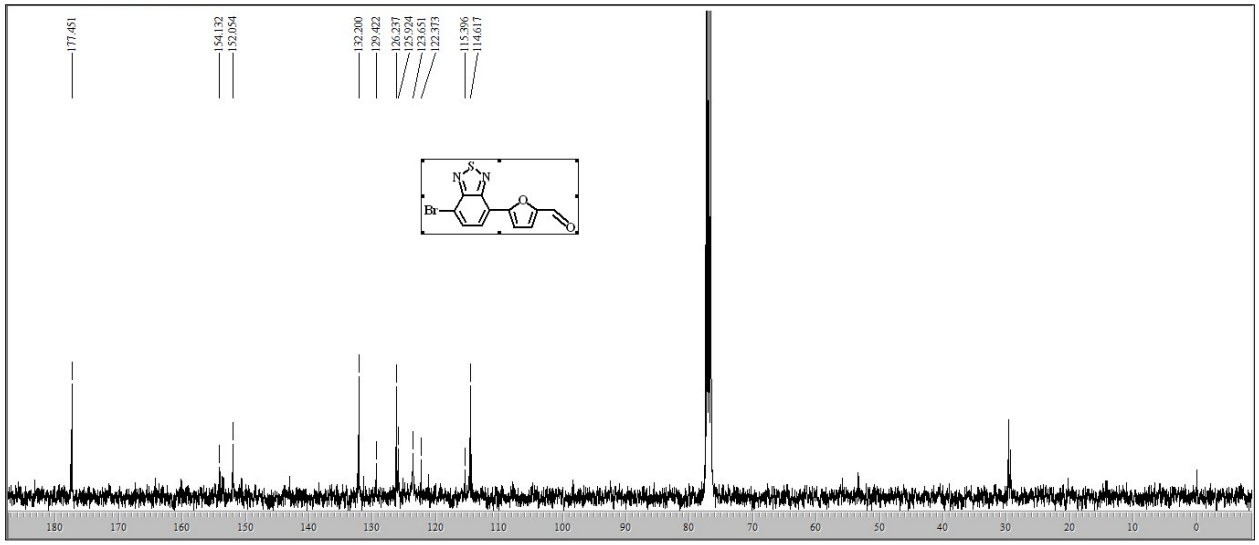

Figure S2. ^{13}C NMR of BT-F-CHO in $CDCl_3$.

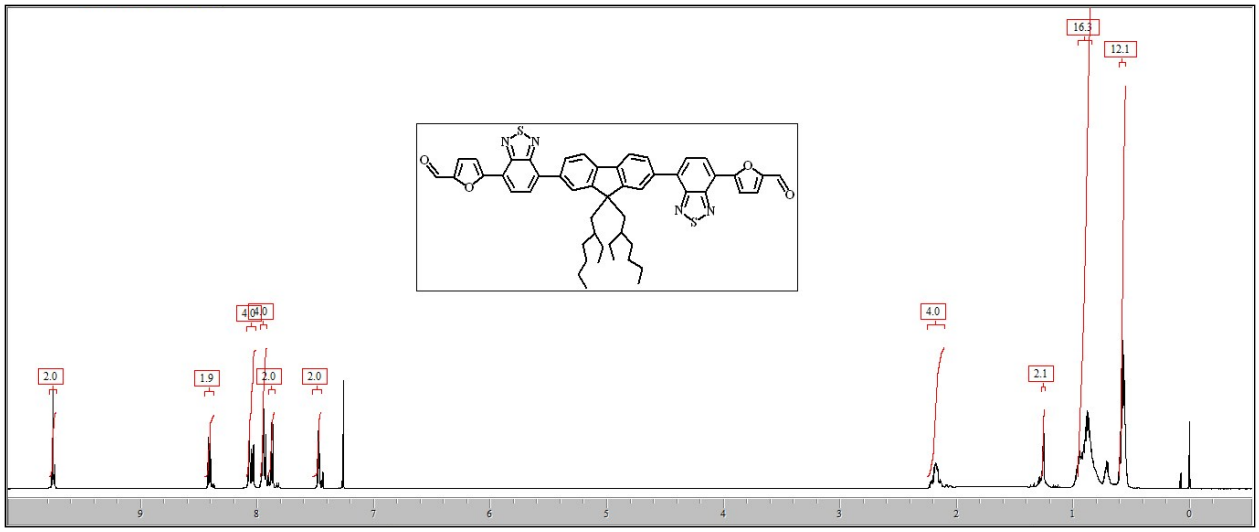

Figure S3. ^{1}H NMR of F2CHO in $CDCl_3$.

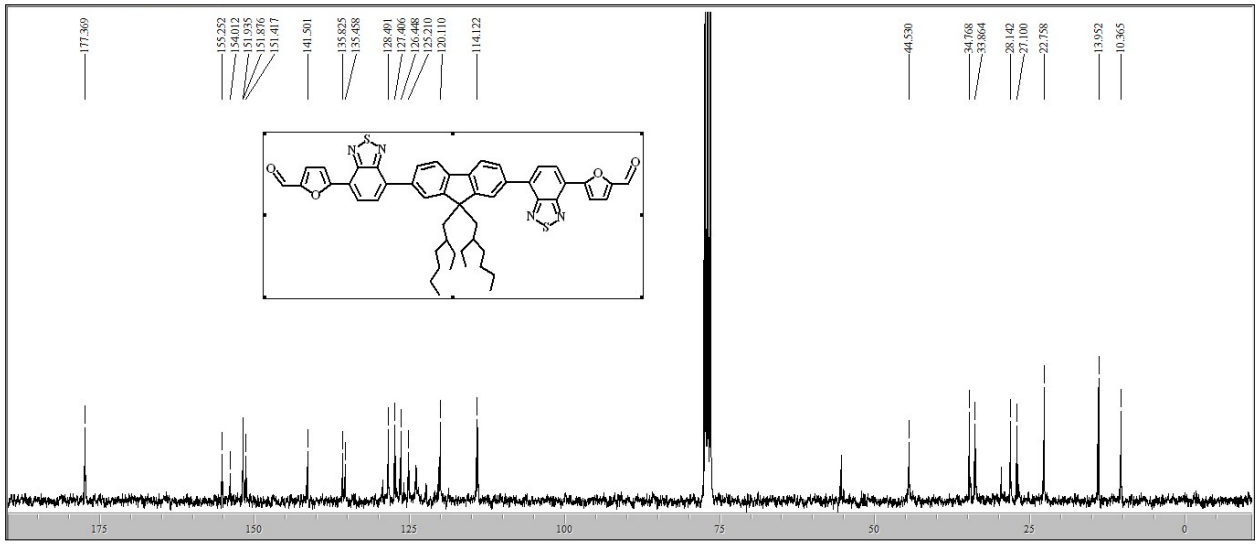

Figure S4. ^{13}C NMR of F2CHO in $CDCl_3$.

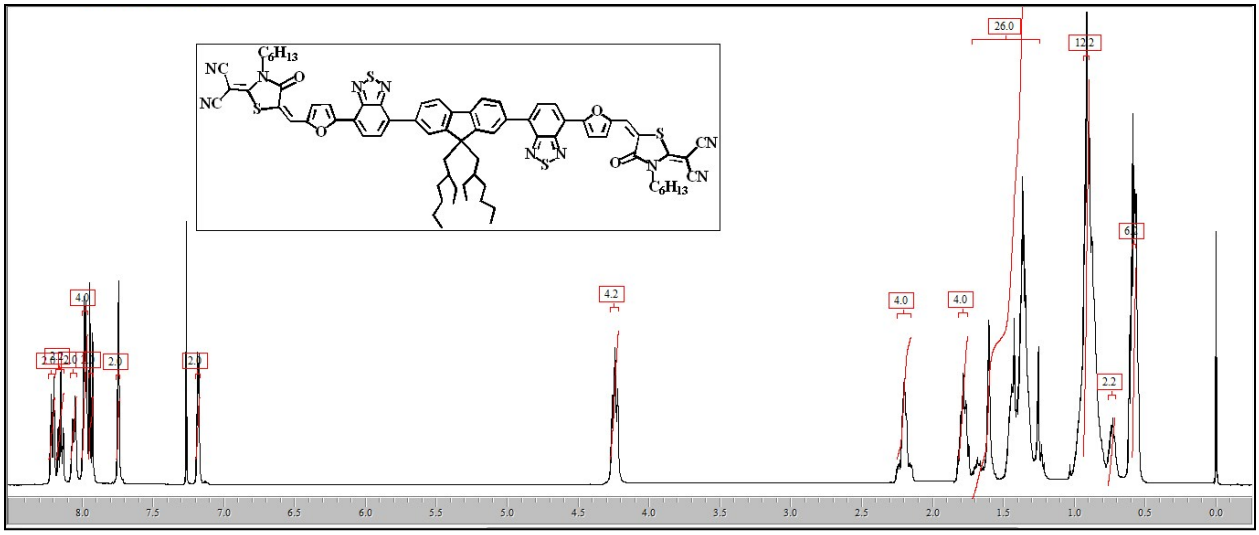

Figure S5. ^{1}H NMR of **FRdCN$_2$** in $CDCl_3$.

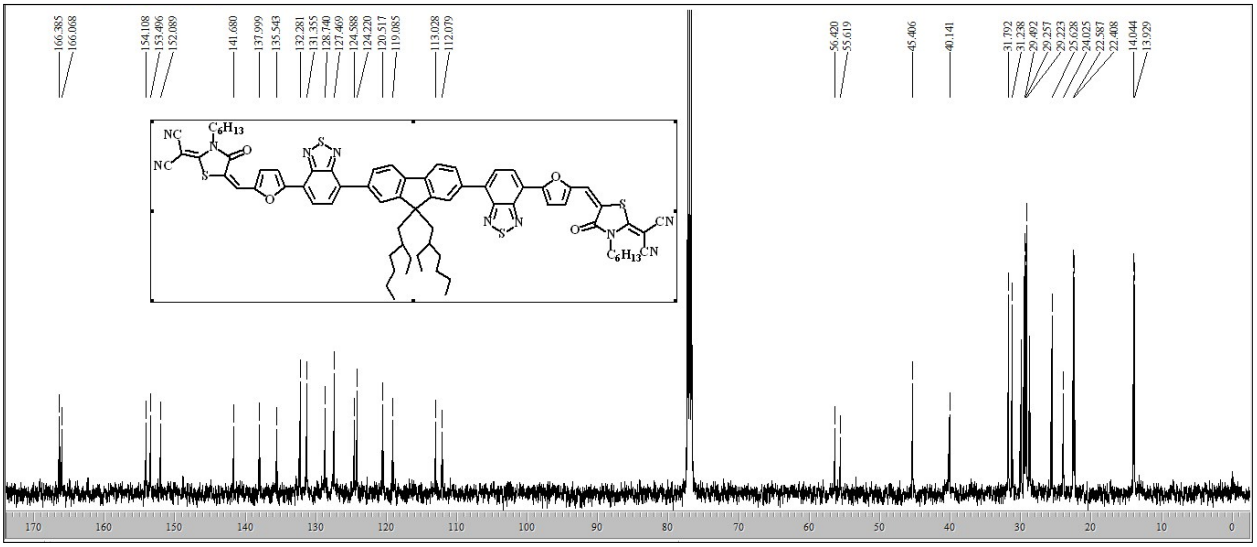

Figure S6. ^{13}C NMR of **FRdCN$_2$** in $CDCl_3$.

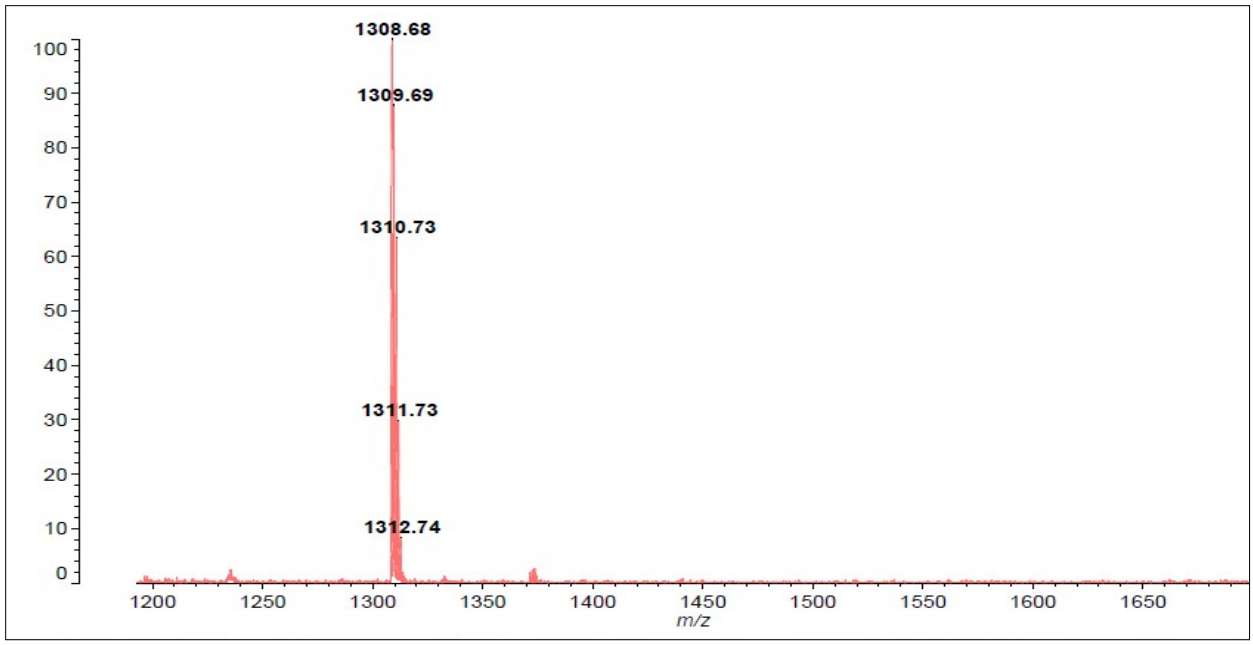

Figure S7. MALDI-TOF spectra of **FRdCN$_2$**.

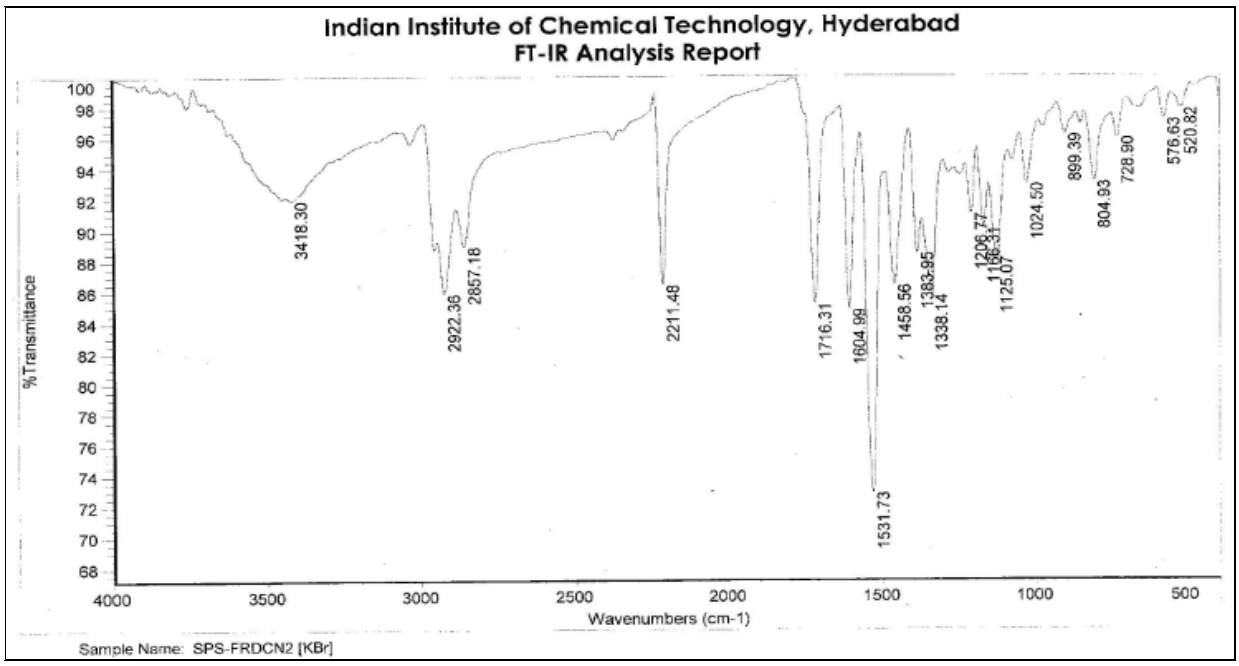

Figure S8. FT-IR spectra of **FRdCN$_2$**.

Table S1. Performance of earlier reported fluorene core based small molecule non-fullerene acceptors.

S.No.	Donor	NFAs	Linker	λ_{max} (nm)	J_{sc} (mA/cm^2)	V_{oc} (V)	FF (%)	PCE (%)
1	P3HT	PMI-F-PMI	-	533	5.28	0.97	41	2.14
2	P3HT	F8DPPTCN	-	643	6.25	0.97	39	2.37
3	P3HT	DPP1	-	599	2.42	1.10	45	1.2
4	P3HT	Flu-IN	Thiophene	518	3.4	0.92	42	1.32
5	P3HT	FLU-RH	Thiophene	500	5.70	1.03	52	3.08
6	P3HT	FLU-ECA	Thiophene	460	2.82	1.03	44	1.26
7	PTB7-Th	DICTF	Thiophene	587	16.3	0.85	55	7.93
8	DR3TSBDT	DTBTF	Thiophene	540	7.42	1.15	45	3.84
9	P3HT	FBR	Benzothiadiazole	488	7.95	0.82	63	4.11
10	PTB7-Th	FBM	Benzothiadiazole	486	11.2	0.88	51	5.1
11	PffBT4T-2OD	BAF-2HDT	Benzothiadiazole	509	14.6	0.77	0.64	7.13
12	PffBT4T-2OD	BAF-4CN	Benzothiadiazole	498	15.52	0.769	70.7	8.4

S3. UV-visible absorption

The UV-Vis absorption spectrum was measured in chloroform ($CHCl_3$) solution on a UV-1601 Shimadzu UV-visible spectrometer. For UV-Vis absorption spectrum measurement in solution, concentrated solution (0.1 mol·L^{-1}) was prepared independently, which was further diluted to get around 0.03 mol·L^{-1} concentrated solution. The absorption spectrum of the dilute solution was recorded and the data point of the absorbance at a certain wavelength *vs.* concentration was then plotted. A good linear relationship was found for acceptor molecule. To measure thin film absorption spectra, glass substrates (1″ × 1′) were thoroughly cleaned in soap solution and untra-sonicated in de-ionized water and acetone sequentially for 15 min in each step and dried. To measure thin film spectrum of two acceptors concentrated solutions (15 mg/ml) in chlorobenzene

were prepared by ultra-sonication for 10 minutes and spin-coated to clean and dry substrate at 800 rpm for 1 min. The absorption spectrums of acceptor molecules were recorded and the data points of the absorbance at a certain wavelength vs. concentration were then plotted.

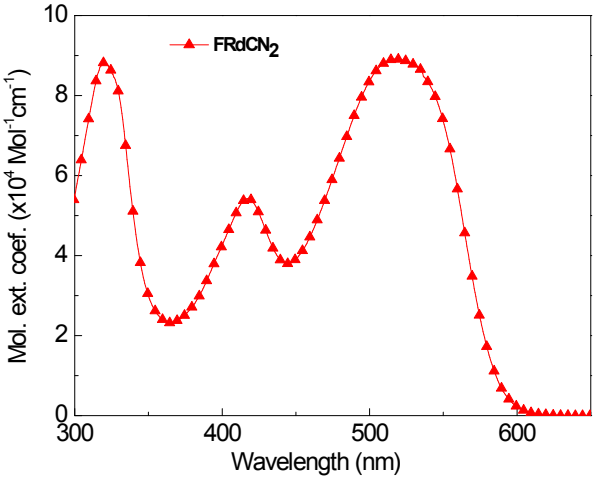

Figure S9. Molar extinction coefficient (ε) of **FRdCN$_2$** in chloroform solution.

S4. Cyclic-voltammetry

Electrochemical properties of **FRdCN$_2$** was investigated by cyclic voltammetry using a conventional three-electrode cell consisting of a cylindrical platinum working electrode, platinum mesh counter electrode and Ag/Ag+ reference electrode was in saturated KCl, calibrated against ferrocene as standard. All CV measurements were carried out at room temperature under nitrogen atmosphere. The electrochemical cyclic voltammetry was performed in a 0.1 mol·L^{-1} tetrabutylammonium perchlorate (TBAP)/dichloromethane (DCM) solution with a scan speed of 0.1 V·s^{-1}. The surface was polished before use. A ferrocene/ferrocenium (F_c/F_c^+) redox couple was used as an external standard. CV measurement was carried out on the acceptor (3×10^{-4} M) in anhydrous and deoxygenated dichloromethane with 0.1 M of tetrabutylammonium perchlorate (TBAP) as the supporting electrolyte. HOMO energy levels measured from onset oxidation potentials and LUMO energy levels were calculated from optical band gap, estimated

from onset absorption spectrums in solution. The cyclic-Voltammogram are shown in **Figure S10**.

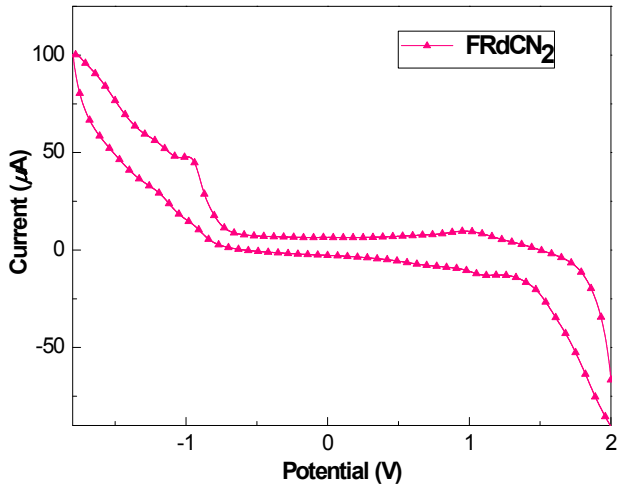

Figure S10. Cyclic Voltammogram of **$FRdCN_2$** in DCM solution.

Table S2. Optoelectronic properties of $FRdCN_2$.

Molecule	E_{HOMO} (eV)	E_{LUMO} (eV)	$E_{0\text{-}0}$ (eV)	λ_{max} (nm) (solution)	λ_{max} (nm) (film)	ε ($Mol^{-1}\cdot cm^{-1}$)
$FRdCN_2$	-5.88	-3.81	2.07	522	530	8.9×10^4

S5. Solar cell deice fabrication

The OPV cells were fabricated in inverted device architecture – Glass/ITO/ZnO/PTB7-Th:SMNFEA/MoO_3/Ag. Pre-patterned ITO coated glass substrates were thoroughly cleaned by ultra-sonication in detergent, deionized water, acetone and isopropanol sequentially for 15 min in each step and dried under flow of dry nitrogen. The prepared ZnO sol-gel was spin-coated on the ITO-coated glass substrate with 3000 rpm. The ZnO films were annealed at 200 °C for 1 h in the air. The thickness of ZnO film is approximately 30 nm, determined by a profilometer. The optimized solution of PTB7-Th:**$FRdCN_2$** (1:1.5 weight ratio, 25 mg/mL in total weight concentration) in CB + additive (1%) was spin casted at 1500 rpm resulting in an active layer

thickness of 120 nm. About 10 nm thick electrons blocking layer of MoO_3 was then thermally evaporated and finally 100 nm silver (*Ag*) was deposited to form the anode. The devices were encapsulated in N_2 filled glove box for future characterizations.

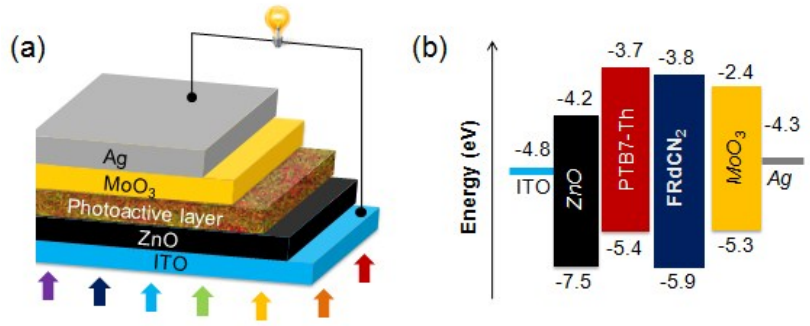

Figure S11. (a) Device structure of fullerene-free BHJ OSC fabricated in this work and (b) energy level diagram corresponding to OPV device under investigation.

S6. Photovoltaic performance

Spectral response measurements were carried out on the OPV devices fabricated from new SMNFEAs with respective additive and annealing treatments in order to investigate photon-to-electron conversion processes in those devices. As shown in **Figure 5a** and **b**, the spectral response curves of PTB7-Th:**FRdCN$_2$** based devices exhibited a very high external quantum efficiency (EQE) value and strong photo response from 400 to 710 nm. The OPV device fabricated from PTB7-Th:**FRdCN$_2$** using CN as additive and TA treatment exhibited maximum EQE of 74% at 530 nm and the EQE value was achieved up to 80% with SVA treatment of active layer. The higher EQE values of PTB7-Th:**FRdCN$_2$** based OPV devices indicating the efficient photon-to-current conversion efficiency of PTB7-Th:**FRdCN$_2$**.

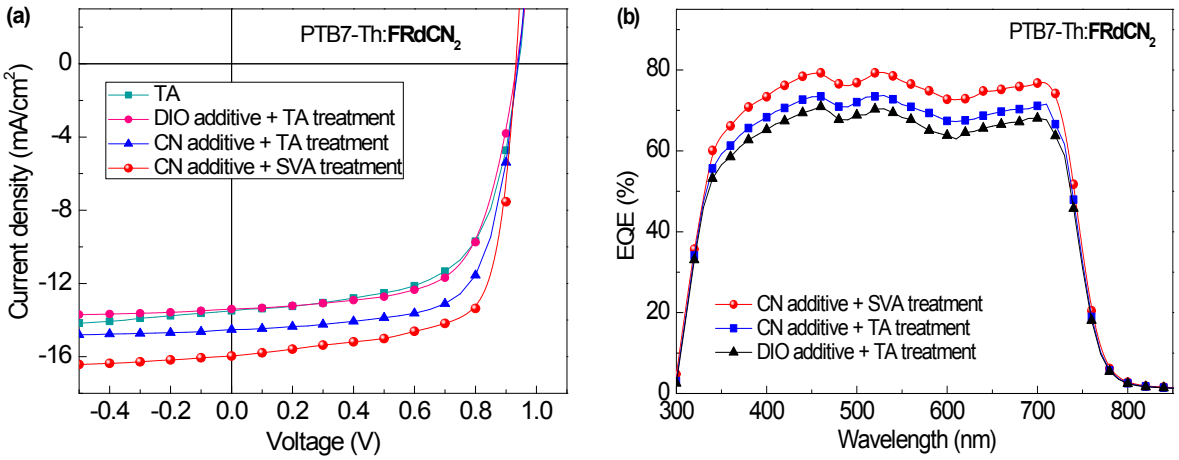

Figure S12. (a) The light J-V characteristics of PTB7-Th:**FRdCN$_2$** based devices, (b) the external quantum efficiency spectra of PTB7-Th:**FRdCN$_2$** based solar cells fabricated under different conditions.

Table S3. Summary of device parameters of polymer organic solar cells based on PTB7-Th:FRdCN$_2$ blend film in different conditions.

SMNFEAs	Additive	Treatments	J_{sc} (mA/cm^2)	V_{oc} (V)	*FF* (%)	*PCE* (%)
	–	As cast[a]	13.1	0.939	58.4	7.2 (6.9)
PTB7-Th: **FRdCN$_2$**	–	TA[a]	13.5	0.941	60.0	7.6 (7.3)
	DIO	TA[a]	13.4	0.936	62.2	7.8 (7.4)
	CN	TA[b]	14.5	0.938	65.3	8.9 (8.7)
	CN	SVA[b]	16.0	0.934	71.9	**10.7 (10.5)**
PTB7-Th: PC$_{70}$BM	DIO	SVA[b]	15.5	0.810	68.7	**8.4 (8.6)**

a = 30 device, b = 50 devices, The numbers mentioned in the parentheses are the average PCEs of the respective category of OPV devices.

In order to check the reproducibility of device performance, at least 30 devices were made for each category from several independent runs. **Figure S13** shows the statistical distribution of 50 such cells made from TA and SVA-treated photo-active layers. For SVA-treated PTB7-Th: **FRdCN$_2$** based devices, 8 out of 50 cells show the highest PCE of 10.7%, whereas 13 and 17 cells showed the efficiency of 10.6 and 10.5%, respectively. In the case of TA-treated OPV

devices, 5 out of 5 cells exhibited maximum PCE of 8.9%, whereas 10 and 20 cells demonstrated a PCE of 8.8 and 8.7%, respectively. The high reproducibility of device results is an indication of stable device fabrication process and reliability of component molecules.

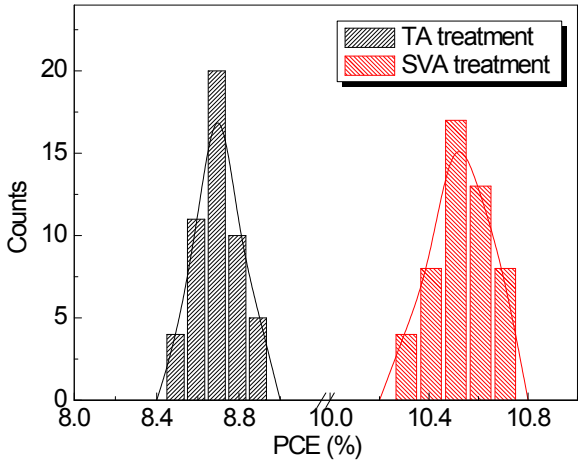

Figure S13. The PCE histograms for TA and SVA-treated PTB7-Th:**FRdCN$_2$** based OSCs made in optimized experimental conditions.

In order to check the durability of the OSCs made with new fullerene-free acceptor **FRdCN$_2$**, devices were regularly tested for about 40 days. In between two consecutive measurements, the encapsulated devices were kept inside plastic boxes and stored in dark. **Figure S14** shows the aging stability data for PTB7-Th:**FRdCN$_2$** based devices in comparison with a standard PTB7-Th:$PC_{70}BM$ based reference solar cell in semi-logarithmic plot. From the figure, it can be seen that the PCE of PTB7-Th:**FRdCN$_2$** has decreased by only 9% over a period of 40 days; whereas for PTB7-Th:$PC_{70}BM$ based solar cells, 26% fall in PCE has been observed for the same duration of time. Hence, it can be inferred that **FRdCN$_2$** based devices are more durable than the benchmark $PC_{70}BM$ based devices.

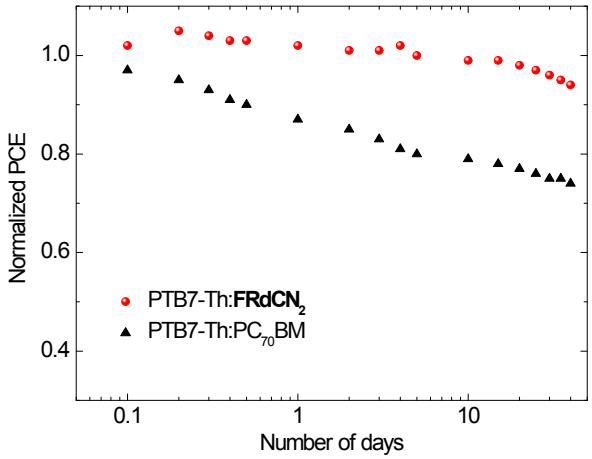

Figure S14. Durability test for optimized PTB7-Th:**FRdCN$_2$** based OSCs in comparison with standard PTB7-Th:$PC_{70}BM$ reference solar cells.

S7. Charge carrier mobility

Dark *J–V* characteristics of ITO/*ZnO*/PTB7-Th:**FRdCN$_2$**/*Al* based electron-only devices and ITO/PEDOT:PSS/PTB7-Th:**FRdCN$_2$**/*Au* based hole only devices treated with thermal annealing and solvent vapor annealing are shown in **Figure S15.** The curves are fitted with Mott–Gurney's SCLC model (continuous lines). The hole mobility of PTB7-Th and electron mobility $FRdCN_2$ in blend are found to be higher in case of SVA treated films compared to that of thermally annealed films**.** The mobility values (μ) are calculated by Mott-Gurney's space charge limited current (SCLC) model,

$$J_{SCLC} = \frac{9}{8}\varepsilon_o\varepsilon_r\mu\frac{V^2}{d^3} \qquad \text{(S1)}$$

where ε_o is the free space permittivity, ε_r is the average relative dielectric constant of the blend film and generally taken as 3, and d is the film thickness.

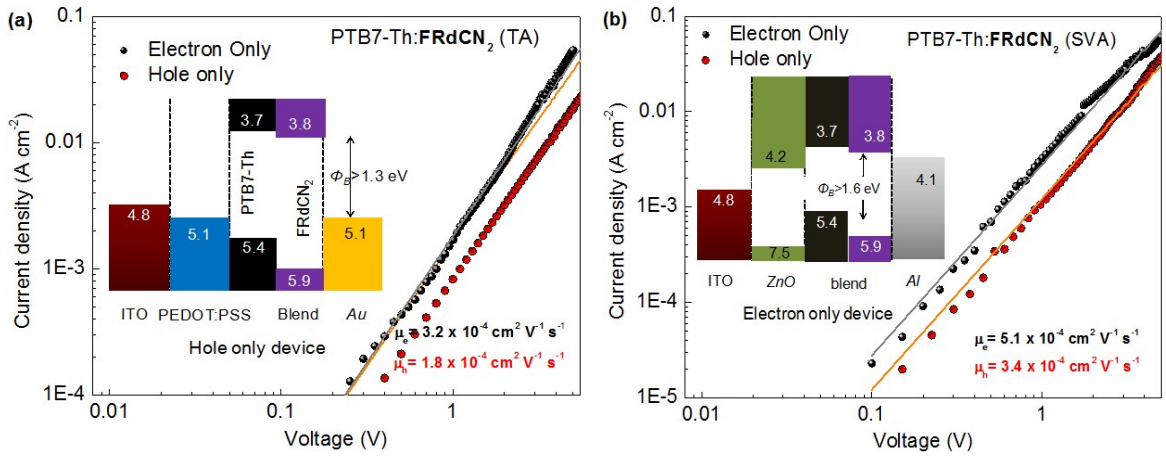

Figure S15. Mott-Gurney's SCLC fitting to calculate hole and electron mobility of PTB7-Th and **FRdCN$_2$** in (a) thermally annealed and (b) solvent vapor annealed films.

Table S4. Charge transport parameters of blend films.

Blends	Treatments	μ_h ($cm^2v^{-1}s^{-1}$)	μ_e ($cm^2v^{-1}s^{-1}$)	Ratio
PTB7-Th:**FRdCN$_2$** (CN)	TA	1.8×10^{-4}	3.2×10^{-4}	1.77
PTB7-Th:**FRdCN$_2$** (CN)	SVA	3.4×10^{-4}	5.1×10^{-4}	1.50

S8. Photoluminescence Quenching

Photoluminescence quenching experiments were carried out on blend film and pristine donor and acceptor film to examine the quenching of PTB7-Th with new acceptor molecules. As shown in **Figure S16**, for PTB7-Th:**FRdCN$_2$** blend film, donor and acceptors photoluminescence are strongly quenched indicating the efficient excitons separation. For blend film of PTB7-Th:**FRdCN$_2$** with a ratio of 1:1 and 1:2.5 the photoluminescence is quenched up 58 and 87%, respectively. The Stern-Volmer quenching coefficient (K_{sv}) has been calculated using the following relation,

$$\frac{\eta_o}{\eta} = 1 + K_{sv}c \qquad \text{(S2)}$$

where η and η_o are emission efficiency in presence and absence of quenchers, respectively, and c is the quencher concentration.

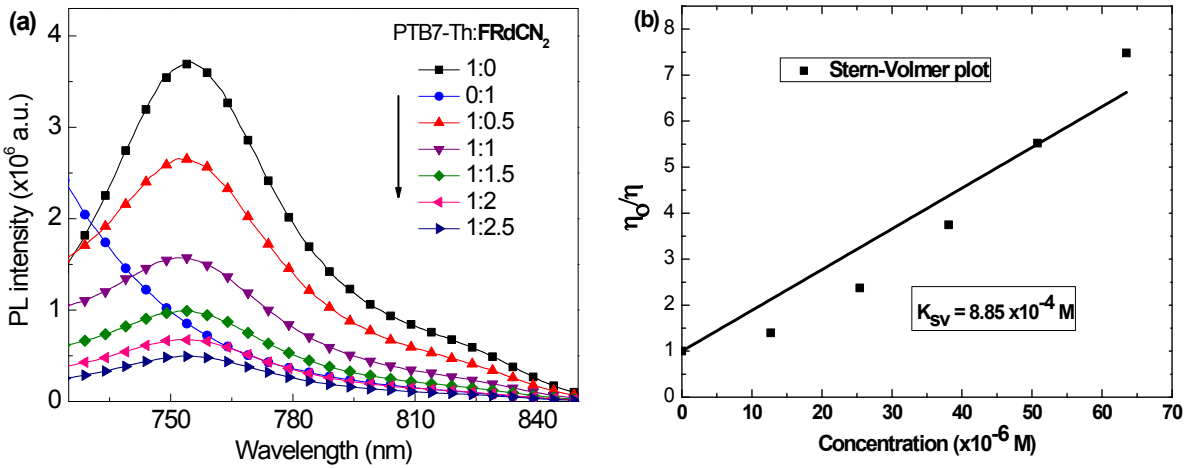

Figure S16. (a) Photoluminescence quenching spectra and (b) Stern-Volmer plots for PTB7-Th:**FRdCN$_2$** blends obtained from PL quenching experiments.

S9. GIXRD analysis

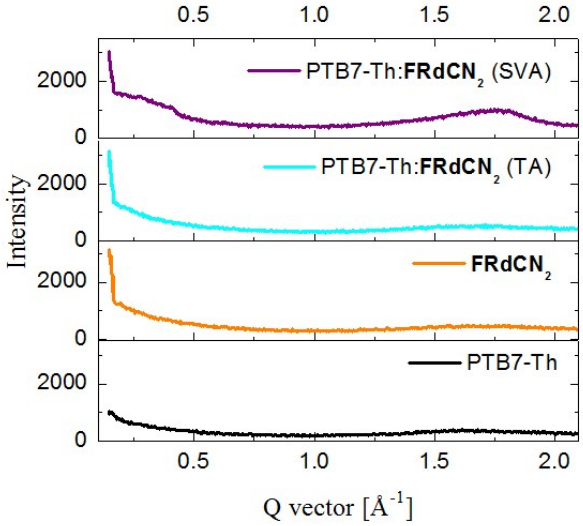

Figure S17. The GIXRD graphs of thermally annealed and solvent vapor annealed PTB7-Th:**FRdCN$_2$** blend film and pristine PTB7-Th and **FRdCN$_2$** films.

Two-dimensional (2D) grazing-incidence X-ray diffraction (GIXRD) technique was used to investigate micro-structural features of pure acceptor molecules and blend film of acceptor with PTB7-Th donor. **Figure S17** represents GIXRD spectra of pristine and blend films.

REFERENCES

1. (a) S. Higashijima, H. Miura, T. Fujita, Y. Kubota, K. Funabiki, T. Yoshida and M. Matsui, *Tetrahedron*, 2011, **67**, 6289-6293; (b) B. A. D. Neto, A. S. A. Lopes, G. Ebeling, R. S. Gonçalves, V. E. Costa, F. H. Quina and J. Dupont, *Tetrahedron*, 2005, **61**, 10975-10982; (c) C. Lavanya Devi, K. Yesudas, N. S. Makarov, V. Jayathirtha Rao, K. Bhanuprakash and J. W. Perry, *J. Mater. Chem. C*, 2015, **3**, 3730-3744; (d) X. Liu, R. Zhu, Y. Zhang, B. Liu and S. Ramakrishna, *ChemComm*, 2008, **28**, 3789-3791.